ASCE-ASME Journal of Risk and Uncertainty in Engineering Systems Part B: Mechanical Engineering
Online journal at:
asmedigitalcollection.asme.org/risk

Qingsheng Wei
College of Engineering,
Shantou University,
243 Daxue Road, Jinping District,
Shantou, Guangdong 515063, China

Peng Chen[1]
College of Engineering,
Shantou University,
243 Daxue Road, Jinping District,
Shantou, Guangdong 515063, China
e-mails: pengchen@alu.uestc.edu.cn;
dr.pengchen@foxmail.com

Jia Gao
College of Engineering,
Shantou University,
243 Daxue Road, Jinping District,
Shantou, Guangdong 515063, China

Ruijin Zhang
College of Engineering,
Shantou University,
243 Daxue Road, Jinping District,
Shantou, Guangdong 515063, China

Changbo He
College of Electrical Engineering and Automation,
Anhui University,
No. 3 Feixi Road, Shushan District,
Hefei, Anhui 230039, China

Junyu Qi
Electronics and Drives,
Reutlingen University,
Alteburgstraße 150,
Reutlingen 72768, Germany

EKBD-MK: Entropy-Kurtosis Bilateral Discernment With Maximum Kurtosis Blind Deconvolution for Fault Diagnosis in Wind Turbine Systems

Wind turbines, as critical components of renewable energy systems, face significant challenges in maintaining operational reliability due to their bearing systems operating under challenging mechanical and environmental conditions. These conditions are further complicated by transient events generating sudden mechanical impulses and persistent harmonic noise from mechanical resonance, which obscure early indicators of component degradation and hinder fault detection. To address these challenges, this research proposes entropy-kurtosis bilateral discernment with maximum kurtosis blind deconvolution (EKBD-MK), a novel diagnostic framework that systematically suppresses nonstationary transient disturbances and irrelevant harmonic components in vibration signals. By employing a Shannon entropy-based noise quantification approach alongside physical interpretations of center frequencies, the proposed method ensures robustness in complex noise environments. Additionally, a signal decomposition strategy through variational mode decomposition (VMD) is developed with an entropy-frequency dual-constraint system to optimize fault information concentration, prevent feature loss, and maintain signal integrity. To further enhance diagnostic accuracy, an adaptive blind deconvolution (BD) strategy incorporating multicomponent preservation and spectral kurtosis (SK)-based enhancement of fault features is implemented, ensuring parameter insensitivity and effective noise suppression. Experimental validation through real case study demonstrates the efficacy of this framework, significantly improving diagnostic precision compared to current methods.
[DOI: 10.1115/1.4069528]

Keywords: wind turbine, signal processing, transient events, fault diagnosis, prognostics health management

1 Introduction

Wind turbines, as sophisticated electromechanical systems that play a critical role in renewable energy generation, present unique operational challenges that demand constant monitoring and maintenance. Their dependable performance relies heavily on the structural and functional integrity of critical components within their transmission chain, with particular emphasis on the bearing systems that facilitate mechanical movement [1–4]. Moreover, these essential bearing components are subjected to extraordinarily demanding operational conditions, encompassing not only severe environmental stressors such as temperature fluctuations and moisture exposure but also constantly varying rotational speeds and mechanical loads. These challenging circumstances create a complex diagnostic landscape where fault identification becomes increasingly intricate. Furthermore, the situation is exacerbated by transient events that generate sudden mechanical impulses, coupled with persistent harmonic noise emanating from mechanical resonance phenomena, which effectively mask subtle early indicators of component degradation. Although the reported diagnostic methodologies have been widely implemented across the industry, they frequently demonstrate significant limitations when confronted with complex noise patterns and dynamic operational environments. These traditional approaches often prove inadequate in extracting and identifying crucial fault features amidst the challenging conditions inherent to wind turbine operations. Consequently, there exists a pressing need for the development and implementation of more sophisticated, robust, and adaptive diagnostic frameworks that can ensure precise fault detection and classification across a broad spectrum of variable operating conditions [5].

In the field of bearing fault diagnosis, the identification of damage-related signals—such as those caused by fatigue, cracking, and wear—is of critical importance. These signals typically manifest as recurring impulse features in the time domain and as

[1]Corresponding author.

Manuscript received June 8, 2025; final manuscript received July 23, 2025; published online March 5, 2026. Assoc. Editor: Ke Feng.

characteristic frequency components in the frequency domain, which are directly related to the specific geometrical and structural properties of the bearing elements [5–7]. Traditional diagnostic approaches have relied heavily on time-domain analysis, employing various statistical indicators [8–10] such as waveform factor, margin factor, impulse factor, and kurtosis. These metrics serve as valuable tools for detecting impulsive or nonstationary vibration features that often indicate fault conditions. However, a significant limitation of these time-domain indicators lies in their susceptibility to operational variations, particularly changes in load and speed conditions, which can compromise their diagnostic reliability. To overcome these limitations, modern diagnostic methodologies have expanded into more sophisticated analytical domains, specifically the frequency and time–frequency domains, which offer enhanced diagnostic capabilities. A particularly noteworthy advancement in this field has been the development and implementation of spectral kurtosis (SK) [11]. This second-order statistical tool [12], designed specifically for nonstationary signal analysis, has gained considerable traction in the diagnostic community. Unlike conventional kurtosis calculations, SK's distinctive approach maps impulsiveness into the frequency domain, providing a more nuanced mechanism for highlighting fault-related frequency components and enabling earlier fault detection.

The inherent constraints of the Kurtogram regarding computational performance and resolution precision have prompted the development of several enhanced methodologies. A notable advancement emerged with the Fast Kurtogram [13], which implements finite impulse response (FIR) filters, achieving substantial reduction in computational demands while maintaining signal integrity. This approach demonstrates computational complexity on par with the fast Fourier transform, facilitating its adoption in industrial contexts. Subsequent innovations by Lei et al. [14] advanced the field by substituting the short-time Fourier transform with wavelet packet transform, thereby achieving superior transient feature detection in noise-contaminated signals through enhanced time–frequency localization and multiresolution analytical capabilities. This foundation was further expanded by Li et al. [15], who synthesized time-domain and frequency-domain spectral negentropy with multiscale decomposition and hierarchical clustering techniques. Their integrated approach enables both efficient detection of recurring transient elements and optimized bandwidth determination.

More recent advances include Autogram [16], which exploits second-order cyclostationarity in bearing signals. Instead of analyzing raw time-domain kurtosis, it computes the kurtosis of the unbiased autocorrelation of the squared envelope, improving upon the traditional Kurtogram. Additionally, entropy-based band selection methods have shown promise. Zhou et al. [17] proposed a hyperbolic tangent fuzzy entropy approach, where wavelet packet energy across bands is normalized, converted into fuzzy sets, and used to identify the most informative frequency components. Yan et al. [18] introduced an entropy maximization-based convex optimization method that automatically locates fault characteristic frequencies in the normalized square envelope spectrum, highlighting the effectiveness of entropy-driven optimization in fault diagnosis.

Although these methods offer notable advantages, nonetheless, they encounter considerable limitations when dealing with transient noise and harmonic noise. Specifically, methods based on the SK [11] demonstrate heightened sensitivity to transient noise, thereby often misclassifying nonfault-related disturbances as fault signatures. Furthermore, their reliance on fixed-scale spectral analysis frameworks hampers their ability to differentiate high-kurtosis harmonics from genuine fault characteristic frequencies in the presence of harmonic noise, thus elevating the likelihood of false alarms or missed detections. On the other hand, information entropy-based methods, while improving robustness to complex signals via uncertainty modeling, nevertheless exhibit vulnerability to anomalous entropy value fluctuations under transient noise, which subsequently can result in inaccurate band selection. In addition, these methods face challenges in effectively identifying highly regular harmonic noise.

Fundamentally, blind deconvolution (BD) methods provide a powerful approach for mechanical fault diagnosis by systematically separating the source signal—generated by transient fault impacts—from background noise and transmission path interference. Specifically, through inverse modeling of the signal propagation process, BD effectively recovers weak fault features, particularly under non-Gaussian noise conditions [19]. Initially, McDonald et al. introduced the maximum correlated kurtosis deconvolution, which subsequently enhances periodic transient components by maximizing correlated kurtosis, thereby significantly improving early fault detection [20]. Furthermore, Li et al. [21] proposed cyclostationary blind deconvolution, which not only denoises the signal but also estimates cyclic frequency via envelope autocorrelation, while adaptively optimizing filter length using an improved success–failure search strategy based on the residual autocorrelation energy ratio. Building upon these foundations, Wang et al. [22] developed autocorrelation-based cyclostationary blind deconvolution, which consequently estimates cyclic frequencies using morphological envelope autocorrelation and additionally introduces the performance efficiency ratio to balance deconvolution performance and computational cost through an equal-step search strategy. Concurrently, frequency-domain BD methods have also advanced substantially. In this context, Yi et al. [23] proposed an adaptive generalized morphological filter-based BD method, coupled with block-based blind source separation and frequency-domain sparse component analysis, thus demonstrating robustness in extracting compound faults. Moreover, to address noise sensitivity in vibration and acoustic testing, He et al. [24] introduced maximum Fourier spectral cyclostationarity blind deconvolution. Notably, inspired by cyclostationarity indicators in rotating machinery, this method constructs a Fourier spectral cyclostationarity index specifically tailored for transformer fault detection, hence showing strong engineering applicability.

Nevertheless, both categories of blind deconvolution methods face distinct challenges. On one hand, time-domain BD methods enhance impact features by maximizing metrics like kurtosis; however, they are prone to misidentifying transient noise as fault signals, consequently leading to erroneous filter parameter adjustments. On the other hand, frequency-domain BD methods, while theoretically possessing frequency selectivity, nonetheless encounter significant difficulties because the broadband energy spread caused by transient events can substantially disrupt the spectral structure. Additionally, strong harmonics may dominate the energy distribution, thereby causing the objective function to deviate from the fault frequency. Furthermore, without robust transient detection and spectral weighting mechanisms, frequency-domain methods struggle to accurately locate the fault band, particularly in scenarios with dense multiple harmonics.

The current reported fault diagnosis techniques suffer from inherent complexity and limitations, as they are particularly sensitive to operational parameters and demonstrate insufficient robustness against transient and harmonic noise. To this end, this research proposes a new method that systematically suppresses both irrelevant periodic harmonic components and nonstationary transient disturbances directly associated with vibration signals. Specifically, this research proposed a novel noise suppression framework that quantifies harmonic noise impact through Shannon entropy while integrating physical interpretation of center frequencies, thereby establishing a robust methodology for complex noise environments that fundamentally overcomes the limitations of traditional approaches. Additionally, this research developed an advanced variational mode decomposition (VMD) control mechanism implementing an entropy-frequency dual-constraint system, where the proposed approach initially employs VMD of the signal; subsequently, guided by prior knowledge of the fault characteristic frequency, this mechanism optimizes fault information concentration, prevents feature loss through insufficient decomposition, and maintains signal integrity via adaptive threshold control of

decomposition levels. Furthermore, modes whose energy is not concentrated around this frequency are systematically eliminated, and Shannon entropy is utilized to refine the remaining modes effectively since the disruptive effect of harmonic noise on the energy structure within certain frequency bands—manifested as significant fluctuations in Shannon entropy—serves as a reliable indicator for identifying and eliminating noisy modes. Moreover, this research established an enhanced blind deconvolution strategy incorporating multicomponent preservation that eliminates parameter sensitivity and ensures reliable performance independent of harmonic frequency identification; consequently, for the retained modes, a frequency-domain blind deconvolution method based on maximum spectral kurtosis is introduced to enhance fault features in the amplitude spectrum, thus significantly improving diagnostic accuracy compared to conventional methods and ensuring that only those modes containing the most fault-relevant information and minimal noise are retained.

The principal contributions of this work are summarized as follows:

(1) This research proposed a novel noise suppression framework that quantifies harmonic noise impact through Shannon entropy while integrating physical interpretation of center frequencies, thereby establishing a robust methodology for complex noise environments that fundamentally overcomes the limitations of traditional approaches.
(2) This research developed an advanced VMD control mechanism implementing an entropy-frequency dual-constraint system that optimizes fault information concentration, prevents feature loss through insufficient decomposition, and maintains signal integrity via adaptive threshold control of decomposition levels.
(3) This research established an enhanced blind deconvolution strategy incorporating multicomponent preservation that eliminates parameter sensitivity and ensures reliable performance independent of harmonic frequency identification, thus significantly improving diagnostic accuracy compared to conventional methods.

The remainder of this article is systematically organized to present a comprehensive exploration of our proposed methodology and its practical applications. Initially, Sec. 2 establishes the fundamental groundwork by thoroughly describing the basic framework and theoretical foundations of VMD and blind deconvolution, which serve as essential building blocks for our proposed method. Subsequently, Sec. 3 delves into the theoretical underpinnings and methodological innovations of our proposed entropy-kurtosis bilateral discernment with maximum kurtosis blind deconvolution (EKBD-MK) method, where each component and its operational mechanisms are meticulously explained and analytically justified. Furthermore, Sec. 4 presents comprehensive case study that effectively demonstrates the practical implementation and superior performance of our proposed method, particularly focusing on the challenging task of diagnosing bearing faults under complex operating conditions where both transient noise and harmonic noise interferences significantly complicate the measurement data. Additionally, the case study provides valuable insights into the method's robustness and effectiveness in real-world applications. Finally, Sec. 5 synthesizes the key findings, highlights the significant contributions of this research, and presents concluding remarks along with potential future research directions in this domain.

2 Preliminaries

2.1 Blind Deconvolution in Signal Processing and System Identification. Blind deconvolution [8] represents a fundamental yet challenging problem in signal processing and system identification, where the primary objective is to simultaneously recover both the original input signal and the system impulse response when neither is known a priori, utilizing only the observed output signal. This inverse problem finds widespread applications in various fields, including image restoration, communications, and acoustic signal processing [7].

In the mathematical framework, the observed signal y is modeled as the result of a convolution between the input signal x and h denoting the effect of the transfer paths, with the addition of inevitable measurement noise n, which can be expressed as

$$y = x * h + n \tag{1}$$

where * denotes the convolution operation. The fundamental challenge of blind deconvolution lies in simultaneously estimating both x and h from the degraded observation y.

To address this inherently ill-posed inverse problem, researchers [25] have developed various approaches that incorporate reasonable assumptions and prior knowledge about the signal and system characteristics. These assumptions typically include but are not limited to sparsity constraints, statistical independence between the input and the impulse response, smoothness properties, or specific parametric models. By carefully integrating these constraints, the ill-posed problem can be transformed into a well-posed optimization framework that yields meaningful solutions.

2.2 Variational Mode Decomposition. Variational mode decomposition [26] represents an advanced signal processing technique that reformulates the traditional signal decomposition task as a sophisticated variational optimization problem. This method systematically decomposes a complex signal $f(t)$ into a predetermined number of intrinsic mode functions (IMFs) through an iterative optimization process, while simultaneously estimating their respective center frequencies and bandwidths. The mathematical formulation of VMD can be expressed as a constrained variational optimization problem

$$\min_{\{u_k\},\{\omega_k\}} \sum_{k=1}^{K} \left\| \partial_t [\delta(t) * u_k(t) e^{-j\omega_k t}] \right\|_2^2, \text{subject to} \quad f(t) = \sum_{k=1}^{K} u_k(t) \tag{2}$$

where $\{u_k\}$ represents the kth mode component, $\{\omega_k\}$ denotes the center frequencies of the kth mode component, and K indicates the total number of modes. The partial derivative with respect to time is represented by ∂_t, while $||\cdot||_2$ denotes the L_2-norm.

The optimization problem is transformed into an unconstrained form through the introduction of a Lagrange multiplier and a quadratic penalty term. The solution is then obtained iteratively in the frequency domain using the alternating direction method of multipliers, which ensures robust convergence and computational efficiency.

During the iterative optimization process, each mode component adaptively updates its center frequency and corresponding bandwidth within the permissible frequency range. This results in a set of IMFs, each precisely localized within a specific frequency band and characterized by a distinct center frequency, thereby providing a comprehensive and physically meaningful decomposition of the original signal.

3 The Proposed Entropy-Kurtosis Bilateral Discernment With Maximum Kurtosis Blind Deconvolution Method

This research proposes an entropy-kurtosis bilateral discernment with maximum kurtosis blind deconvolution method diagnostic methodology that synergistically combines two sophisticated analytical components: a comprehensive frequency band screening mechanism that leverages both center frequency analysis and Shannon entropy metrics, alongside a blind deconvolution filter optimized through spectral kurtosis maximization. The multistage screening process systematically evaluates and isolates frequency bands that carry crucial diagnostic information while efficiently eliminating redundant spectral content, thereby substantially

enhancing both computational efficiency and diagnostic precision. Furthermore, the optimized blind deconvolution filter employs adaptive processing techniques to capture subtle yet diagnostically significant fault signatures without requiring a priori knowledge of the signal characteristics, thus markedly improving fault detection reliability. Through the strategic integration of these complementary analytical modules, the framework achieves superior noise suppression capabilities and robust feature extraction, ultimately leading to significantly enhanced sensitivity and reliability in mechanical fault diagnosis applications. The comprehensive architectural design of this proposed approach is illustrated in Fig. 1.

3.1 Frequency Band Analysis: Integration of Entropy-Based Screening and Central Frequency Optimization. Following the application of VMD, the signal is decomposed into multiple IMFs, each representing distinct frequency bands within the original signal. However, the inherent complexity of mechanical systems necessitates careful consideration of several factors: Fault characteristic frequencies typically manifest selectively across specific frequency bands, while various forms of noise and signal complexity can potentially mask or distort fault-related information, thereby complicating subsequent diagnostic analysis. Consequently, it becomes imperative to implement a systematic approach for identifying and isolating the most diagnostically relevant IMFs. This section delineates a novel dual-stage modal screening algorithm designed to distill the initial set of modes into an optimized subset of x modes, where $x \leq n_{\text{imf}}$, with n_{imf} representing a user-defined hyperparameter that establishes the upper bound for mode selection.

3.1.1 Spectral-Based Modal Discrimination Through Central Frequency Analysis. In the context of mechanical fault diagnosis, when an IMF's center frequency f_c exhibits proximity to a known fault characteristic frequency f_{fault}, the corresponding time–frequency energy distribution manifests distinctive patterns characterized by periodic impulses and fault-induced modulation phenomena. Such modal components demonstrate enhanced sensitivity to fault-related features, with their waveform envelopes and transient characteristics serving as primary carriers of diagnostic information.

The quantitative determination of an IMF's center frequency f_c is accomplished through comprehensive spectral analysis. Given the kth IMF denoted as $u_k(t)$ and its corresponding Fourier transform $U_k(\omega)$, the center frequency f_{ck} is mathematically expressed through the normalized first moment of the power spectrum

$$f_{ck} = \frac{\int_{-\infty}^{\infty} w|U_k(w)|^2 dw}{\int_{-\infty}^{\infty} |U_k(w)|^2 dw} \tag{3}$$

To mitigate information redundancy inherent in VMD decomposition, we implement a selective filtering criterion whereby modes are retained only if they satisfy the following proximity condition:

$$|f_{ck} - f_{\text{fault}}| \leq \epsilon_f \tag{4}$$

where ϵ_f represents a carefully calibrated threshold parameter.

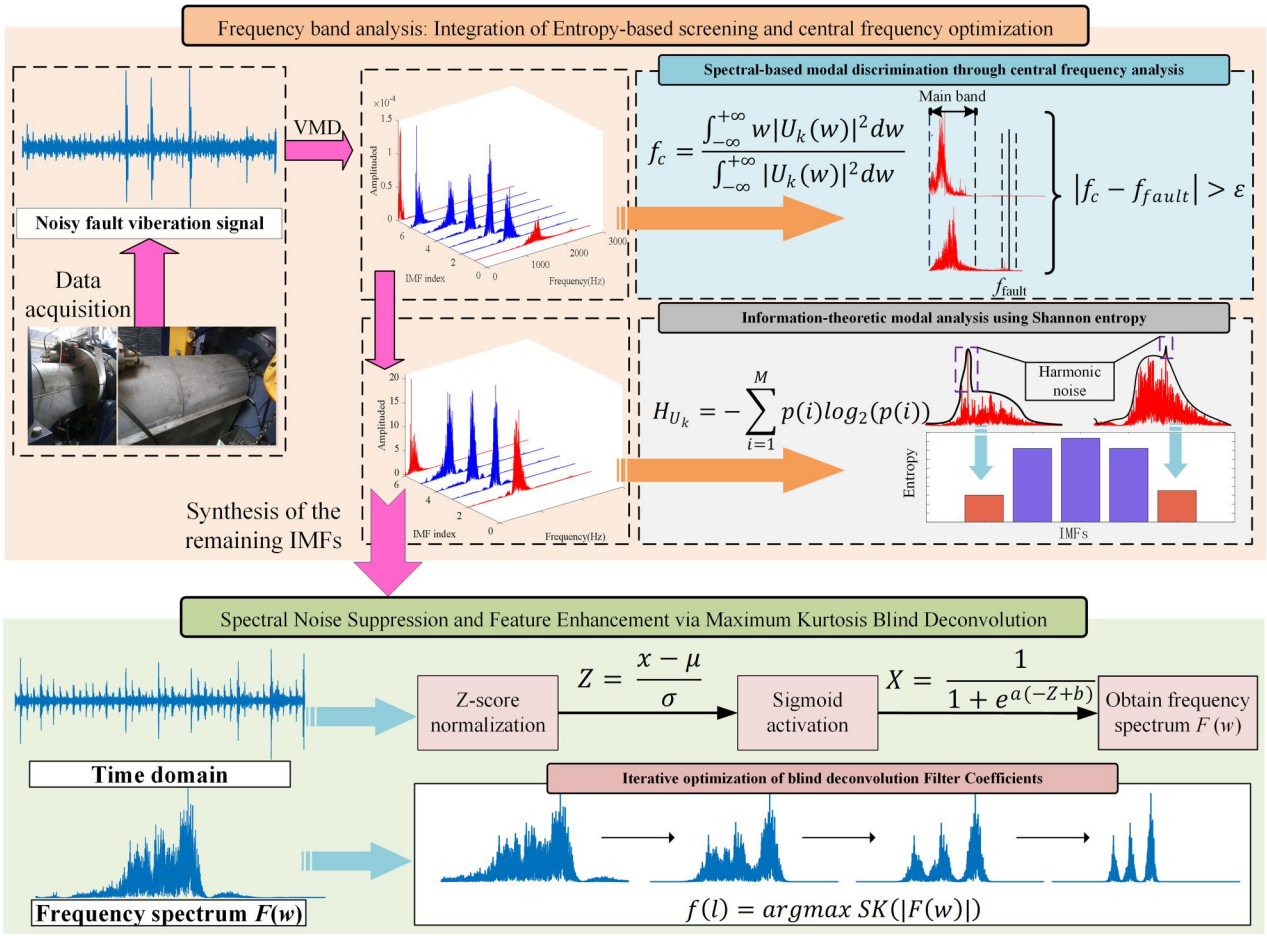

Fig. 1 Proposed framework for entropy-kurtosis based bilateral discrimination and frequency domain blind deconvolution

3.1.2 Information-Theoretic Modal Analysis Using Shannon Entropy. The theoretical foundation of our approach leverages Shannon entropy as a sophisticated measure of information complexity, particularly in its capacity to detect and quantify localized energy concentrations within the frequency domain. Through systematic transformation of time-domain signals into their frequency-domain representations via advanced signal processing techniques such as Fourier or wavelet transforms, we enable comprehensive analysis of underlying frequency components and their distributions. This mathematical framework facilitates precise quantitative assessment of signal complexity through entropy-based metrics, as elaborated in the following methodology.

The analytical process begins with the transformation of the time-domain signal $x(n)$ into its frequency-domain representation using the discrete Fourier transform. By transforming $x(n)$ into its frequency-domain representation denoted as $X(k)$, we enable a comprehensive analysis of underlying frequency components and their distributions.

Let the magnitude spectrum $|X(k)|$ represent the amplitude at each frequency component. We partition the frequency domain into M equal-width intervals and define the probability distribution across these bins as

$$p(i) = \frac{\sum_{k \in \text{bin}\, i} |X(k)|^2}{\sum_{k=0}^{N-1} |X(k)|^2}, \quad i = 1, 2, \ldots, M \tag{5}$$

ensuring that $\sum_{i=1}^{M} p(i) = 1$.

The Shannon entropy is then computed as

$$H(X) = -\sum_{i=1}^{M} p(i) \log_2(p(i)) \tag{6}$$

This formula measures the uncertainty of the frequency distribution. A higher entropy value indicates a more uniform frequency distribution, while a lower value suggests that certain frequencies dominate. To facilitate comparisons between signals, the Shannon entropy is often normalized. The normalized Shannon entropy $H_{\text{norm}}(X)$ is defined as

$$H_{\text{norm}}(X) = \frac{H(X)}{\log_2(M)} \tag{7}$$

3.2 Blind Deconvolution for Noise Reduction and Feature Enhancement. After modal screening, we identify the frequency bands that merit focused analysis. However, at this stage, a major limitation is the heavy dependence on the effectiveness of VMD decomposition. To address this challenge, this paper proposes the design of a blind deconvolution filter f for spectral filtering.

Before applying blind deconvolution in the frequency domain, the reconstructed signal is processed through two time-domain operations. The first operation is signal normalization, which is implemented using Eq. (8). This process scales the signal amplitude to the range $[-1, 1]$, thereby eliminating energy variations caused by changes in operating conditions such as load or speed, and suppressing random amplitude fluctuations due to transient noise. The second operation involves the application of a sigmoid activation function, as defined in Eq. (9). This step constructs a nonlinear feature mapping space; its saturation characteristic enhances the sparse representation of fault impact components while effectively suppressing broadband noise interference

$$z = \frac{x - \mu}{\sigma} \tag{8}$$

where x is the reconstructed signal, μ is the mean of the signal, and σ is the standard deviation of the signal

$$u = \frac{1}{1 + e^{a(-z+b)}} \tag{9}$$

Here, z is the normalized vibration signal, a is the scaling coefficient, and b is the shifting coefficient.

The method proposed in this paper uses activation functions to preprocess the reconstructed time-domain signals. The aim is to balance feature domain energy and enhance fault sparsity, thereby constructing an optimized feature space that significantly improves the ability to distinguish fault features from background noise. Consequently, the amplitude spectrum input into the blind deconvolution filter exhibits more pronounced fault-related characteristics. By maximizing the spectral kurtosis objective function, the energy can be more effectively concentrated on the fault frequency, as the preprocessing process suppresses noise that could distort the spectral structure.

Furthermore, existing similar studies [27,28] indicate that the sigmoid activation function, through its nonlinear mapping, enhances the gradient of small-amplitude fault signals. During the iterative optimization process, this significantly increases sensitivity to early weak impact features or vibration impacts that are drowned out by noise, accelerating the convergence of subsequent iterative algorithms and enhancing stability.

After data preprocessing, we aim to use the principle of deconvolution in the spectral distribution to assist in bearing fault detection through spectral analysis. The primary goal is to optimize the filter f so that the filtered spectral amplitude spectrum Y exhibits significant pulse characteristics while effectively suppressing noise components, thereby achieving noise reduction and feature enhancement. Inspired by the minimum entropy deconvolution method [29], this study employs SK as a measure of sparsity in the blind deconvolution algorithm. The calculation method for spectral kurtosis is as follows:

$$\text{SK} = \frac{\sum_{n=1}^{N} (U(n))^4}{\left(\sum_{n=1}^{N} (U(n))^2 \right)^2}, \quad \text{subject to} \quad U(n) \geq 0 \tag{10}$$

where U is the frequency domain amplitude spectrum of u in Eq. (9). $U(n)$ is the spectral amplitude at index n. N is the length of U. Therefore, the objective function is as follows:

$$\max_{f} \frac{\sum_{n=1}^{N} (U(n))^4}{\left(\sum_{n=1}^{N} (U(n))^2 \right)^2}, \quad \text{subject to} \quad U[n] \geq 0 \tag{11}$$

Assuming that L is the length of filter coefficients f, the process of obtaining the filtered spectrum Y can be expressed by the following formula:

$$\begin{aligned} Y(n) = \hat{f}(l) * U(n) &\leftrightarrows Y(n) = \sum_{l=1}^{L} \hat{f}(l) U(n-l) \\ &\leftrightarrows \frac{\partial Y(n)}{\partial \hat{f}(l)} = U(n-l) \end{aligned} \tag{12}$$

Since we want to maximize the spectral kurtosis of Y, the mathematical relationship between SK and the filter coefficients f can be expressed by the following formula:

$$\frac{\partial \text{SK}\left(\hat{f}(l)\right)}{\partial \hat{f}(l)} = 0 \tag{13}$$

The final expression is as follows:

$$\underbrace{\frac{\sum_{n=1}^{N} Y(n)^2 \sum_{n=1}^{N} Y(n)^3 U(n-l)}{\sum_{n=1}^{N} Y(n)^4}}_{B} = \underbrace{\sum_{m=1}^{L} f(m)}_{f} \underbrace{\sum_{n=1}^{N} U(n-l)U(n-m)}_{A} \tag{14}$$

For simplification, the expression of Eq. (14) can be rewritten in matrix form

$$\Rightarrow B = fA, \quad \Rightarrow f = A^{-1}B$$

$$A = U_0 U_0^{\mathrm{T}}$$

$$B = \frac{\sum_{n=1}^{N} Y(n)^2}{\sum_{n=1}^{N} Y(n)^4} U_0 [Y(1)^3\, Y(2)^3 \ldots Y(N)^3]^{\mathrm{T}}$$

$$U_0 = \begin{bmatrix} U(1) & U(2) & U(3) & \cdots & U(N) \\ 0 & U(1) & U(2) & \cdots & U(N-1) \\ 0 & 0 & U(1) & \cdots & U(N-2) \\ \vdots & \vdots & \vdots & \ddots & \vdots \\ 0 & 0 & 0 & \cdots & U(N-L+1) \end{bmatrix} \tag{15}$$

Therefore, the calculation of filter coefficients can be intuitively expressed as follows:

$$f = \frac{\sum_{n=1}^{N} Y(n)^2}{\sum_{n=1}^{N} Y(n)^4} \left(U_0 U_0^{\mathrm{T}}\right)^{-1} U_0 \left[Y(1)^3\, Y(2)^3 \ldots Y(N)^3\right]^{\mathrm{T}} \tag{16}$$

Equations (12) and (14) provide a comprehensive representation of the convolution operation, wherein each component is systematically processed through elementwise multiplication followed by an aggregative summation. While this theoretical formulation is mathematically elegant, it is pertinent to note that in practical computational implementations and modern software frameworks, convolution operations are predominantly executed through efficient matrix multiplication techniques. Consequently, the equation referenced in Eq. (14) can be methodically decomposed into three fundamental constituent matrices, each serving a distinct mathematical purpose: the filter coefficient matrix f, which encapsulates the convolution kernel parameters; the Toeplitz autocorrelation matrix A, which captures the inherent signal structure and temporal relationships; and the iterative output matrix B, which accumulates the transformed results. Equations (15) and (16) provide a comprehensive explanation of the details of these matrices.

Eventually, as the kurtosis of the filtered amplitude spectrum Y converges during the iteration, we also design a filter to filter out the noise-free amplitude spectrum, where ϵ_{sk} is a hyperparameter

$$|\mathrm{SK}(Y_{k+1}) - \mathrm{SK}(Y_k)| < \epsilon_{\mathrm{sk}} \tag{17}$$

4 Experimental Validation

This section presents and analyzes a thoroughly investigated case study, as detailed in Secs. 4.1 and 4.2, to demonstrate the effectiveness and practical applicability of the proposed diagnostic method. The study addresses the challenging task of identifying and characterizing bearing faults in a wind turbine system under complex operational conditions, including transient interference and harmonic noise components. Insights from this real-world application highlight the method's ability to provide reliable fault diagnosis in engineering practice. To ensure transparency and enable replication by the research community, all critical parameters and operational variables necessary for implementing the proposed algorithm are documented and summarized in Table 1.

Table 1 Summary of parameters employed in the proposed algorithm

Symbol	Description	Value
α	Penalty factor in VMD	6360
k	Total number of IMFs	10
n_{imf}	Number of retained IMFs after selection	3
ϵ_f	Threshold for frequency deviation tolerance	30 Hz
ϵ_{sk}	Convergence criterion threshold	1.2
a	Scaling coefficient of the activation function	182
b	Translation coefficient of the activation function	0

4.1 Test Rig and Data Overview. The proposed fault diagnosis methodology for wind turbine systems, particularly focusing on generator bearing diagnostics, has been validated using real-world vibration data collected from a wind farm located in Lunan, China. The subject of investigation is a 1.5 MW doubly fed induction generator wind turbine system, with its configuration illustrated in Fig. 2.

For condition monitoring purposes, 12 accelerometers were installed at various locations along the drivetrain. This study focuses on data acquired from channel 05, which is positioned at the generator input shaft as shown in Fig. 3(*a*), ensuring the shortest signal transmission path to the monitored bearing. Figures 3(*b*) and 3(*c*) show physical evidence of inner race defects on the rolling bearings.

Wind turbines operate under variable-speed conditions due to fluctuating wind speeds and dynamic loads, presenting significant challenges for reliable fault diagnosis. In this study, special attention is given to data collected at a nominal rotational speed of 1080 rpm, which is considered a critical operating point.

The data acquisition protocol was conducted under the following conditions:

(1) Data were collected semimonthly at a sampling frequency of 20,000 Hz. Fifteen independent datasets were randomly sampled within each 24-h period to ensure comprehensive analysis.
(2) Due to varying meteorological conditions, maintaining an exact rotational speed of 1080 rpm was challenging. Consequently, deviations in data acquisition timing occasionally occurred; these were accounted for during data processing to preserve the integrity of the health monitoring results.

A meticulous examination of the acquired vibration signals, as presented in Fig. 4, reveals two distinct and significant categories of noise interference, each manifesting unique characteristics across both temporal and spectral domains. Within the temporal domain, as evidenced in Fig. 4(*a*), the presence of substantial transient noise is particularly noteworthy, characterized by sudden, ephemeral, pulse-like disturbances. These transient phenomena, predominantly originating from external mechanical impacts or nonperiodic environmental perturbations, present considerable challenges to maintaining the integrity and reliability of subsequent signal analysis procedures.

The frequency domain analysis, as shown in Fig. 4(*b*), presents new challenges and features. In the high-frequency region, the

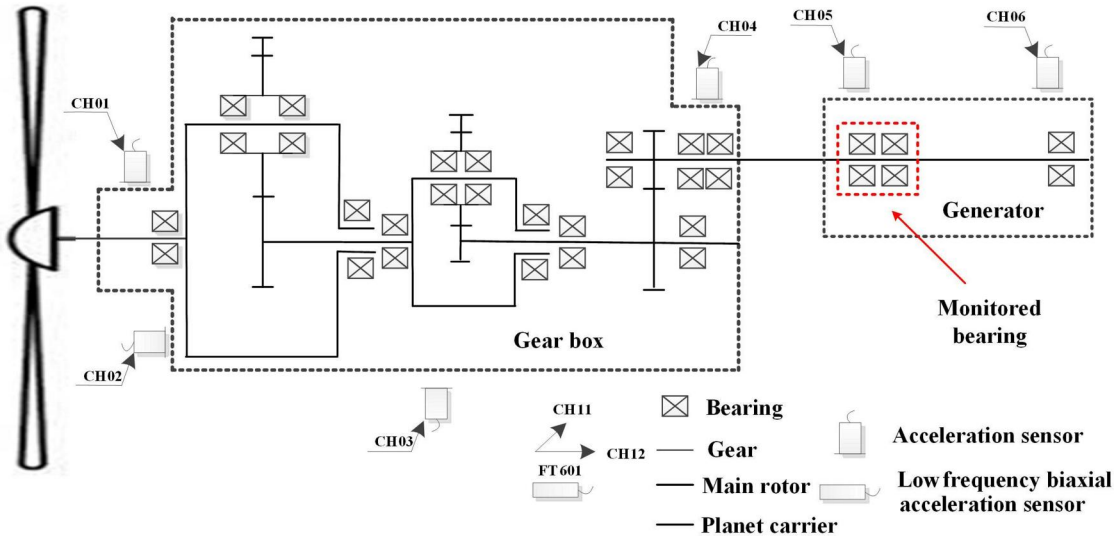

Fig. 2 Structure schematic of the wind turbine system

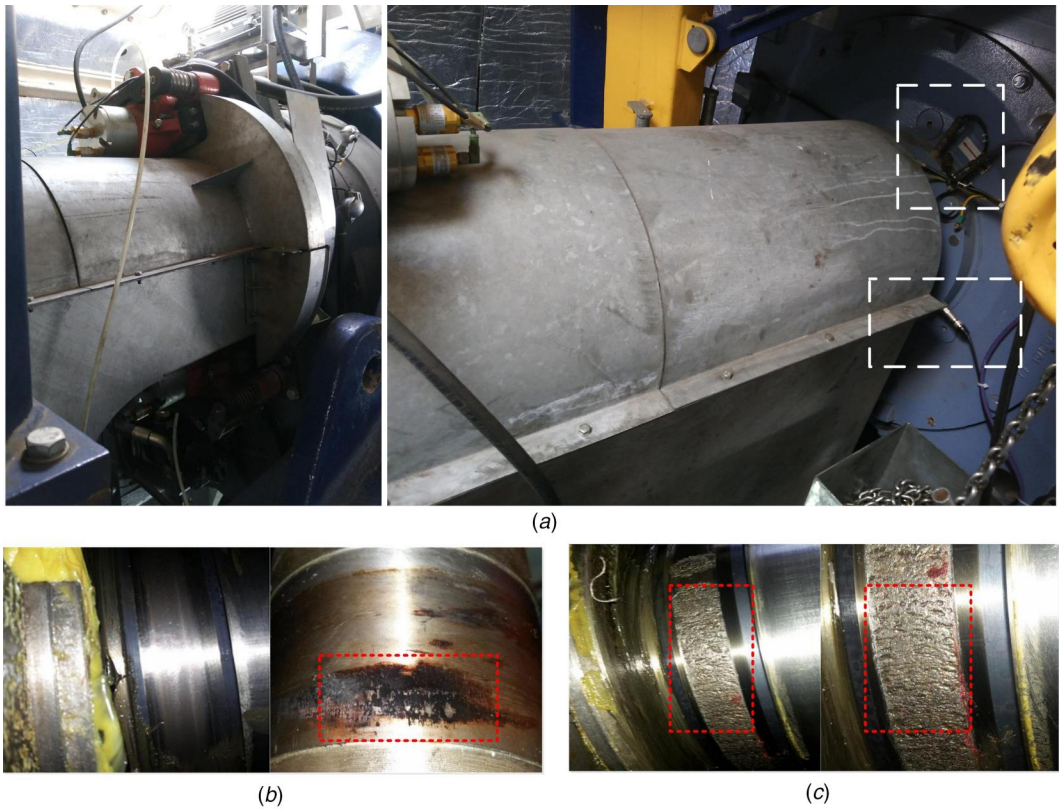

Fig. 3 (*a*) Vibration accelerometer installation locations on the wind turbine generator shown in horizontal and vertical orientations, (*b*) inner race electrical corrosion failure observed in the bearing, and (*c*) worn inner surface of the bearing's inner race

spectrum is clearly divided into distinct bands with characteristic frequencies, but it remains unclear whether these frequencies are related to fault characteristics; conversely, the low-frequency spectrum is primarily composed of harmonic noise. These harmonics typically appear as spectral elements at the fundamental frequency and its integer multiples, often resulting from mechanical defects such as rotational asymmetry, component aging, or inherent system nonlinearity. These harmonics not only degrade the integrity of the original signal but also lead to incorrect condition assessments, as they can mask or mimic true fault characteristics. These characteristics have necessitated configuring the VMD with ten layers to effectively capture the signal's frequency content. However, this parametric configuration introduces certain analytical challenges.

The effectiveness of this decomposition process depends on selecting an appropriate number of layers. Too few layers cause spectral aliasing, mixing fault frequencies with unrelated components and reducing fault detection accuracy. Conversely, too many layers produce unnecessary components and create excessively fine frequency partitions, which obscure signal features. When signal

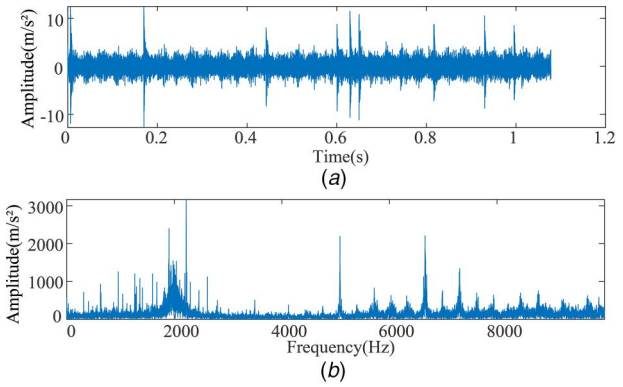

Fig. 4 (*a*) Time domain of the original signal and (*b*) frequency domain of the original signal

information density is low, this results in spurious modes, particularly in high-frequency, low-energy regions unrelated to the actual signal. These artifacts increase computational load and reduce diagnostic precision, highlighting the need to optimize layer selection. Entropy-based analysis methods help assess decomposed frequency structures for optimal layer selection. Selecting IMFs based on entropy reduction principle is essential for accurate fault diagnosis. This approach extracts meaningful signal components, reduces noise and frequency overlap, and improves diagnostic reliability.

4.2 Comparison and Validation of Analysis Results. After VMD decomposition which is shown in Fig. 5(*a*), we filtered out the IMFs that do not concentrate around the fault characteristic frequency, particularly focusing on components in the low-frequency range. As a result, IMF7, IMF8, IMF9, and IMF10 were retained as shown in Fig. 5(*b*), with their center frequencies being 615.082 Hz, 1238.54 Hz, 1888.19 Hz, and 2211.11 Hz, approximately 2 times, 4 times, 6 times, and 7 times the ball pass frequency of the inner ring (BPFI) (319.769 Hz), respectively. The deviation of these center frequencies is within a reasonable range of $\epsilon_f = 30$ Hz. From the retained IMFs, it is evident that some adjacent IMFs have center frequencies differing by about 2 times the BPFI, indicating the limitations of our decomposition levels. In certain frequency bands, VMD performed more detailed segmentation, reflecting the high requirements for precise parameter settings in VMD. Therefore, using the physical prior knowledge of the fault characteristic frequency to screen specific frequency bands for analysis can help avoid information redundancy and feature extraction difficulties.

From the remaining IMFs, it is necessary to extract the fault characteristic frequencies while addressing the challenge that harmonic noise can hinder their identification. In practice, harmonic components represent periodic or repeating patterns that concentrate energy at specific frequencies. In mechanical vibration analysis, such harmonics, often arising from normal machinery rotation, cause pronounced energy concentrations at fixed frequencies and reduce Shannon entropy. When faults occur, they introduce new or altered frequency components, increasing the signal's disorder and complexity, which raises Shannon entropy and indicates fault-related disturbances.

For fault diagnosis, converting signals to the frequency domain and calculating Shannon entropy based on magnitude distributions offers a robust approach to quantifying spectral features and complexity. Calculating entropy in the frequency domain is preferred because of its higher sensitivity to signal-to-noise ratio changes, making it a reliable metric for identifying subtle shifts in energy distribution. Previous studies, such as those on energy detection methods [30], have shown that frequency-domain entropy spectra outperform traditional approaches.

When harmonic noise is present, such as periodic interference or high-amplitude, narrow-band signals, it creates energy peaks in the frequency domain. These peaks can mask important vibration information and significantly lower Shannon entropy, highlighting entropy's value in assessing signal organization. High-energy impacts reduce entropy, as they make the signal more predictable and less complex. For example, an idealized geophysical signal with a few strong, and many weak, reflections shows lower entropy and greater order—a phenomenon confirmed in earlier work [31]. Thus, reducing harmonic noise and evaluating entropy are critical to improving diagnostic accuracy.

Among the four selected IMFs, the normalized Shannon entropy of IMF7, IMF8, IMF9, and IMF10 is 0.576, 0.784, 0.685, and 0.797, respectively. These values reflect the complexity and energy distribution of each IMF. In Table 1, the value of the hyperparameter n_{imf} is set to 3, indicating that we ultimately retain a maximum of three IMFs. IMF7 has the lowest entropy value, suggesting a more ordered structure and less assistance in fault diagnosis. Therefore, IMF7 is excluded as retaining it could hinder the identification of important diagnostic features. After removing IMF7, the fault diagnosis process becomes more robust, as the remaining IMFs better preserve key fault-related features and reduce the impact of harmonic noise.

In the analysis of signal processing outcomes, the time-domain waveform and corresponding frequency spectrum of the reconstructed signal, which was obtained through the superposition of the remaining IMFs, are presented in Figs. 6(*a*) and 6(*b*), respectively. Despite the implementation of selective mode screening procedures, it is noteworthy that substantial noise interference continues to manifest in the signal, necessitating further processing steps. To address this persistent noise issue, the preprocessed amplitude spectrum was subsequently subjected to blind deconvolution analysis.

In the implementation stage, the frequency-domain blind deconvolution framework was executed using an FIR filter with a carefully selected length of 25 samples. This specific parameter selection was strategically chosen to mitigate potential overfitting phenomena, which could otherwise arise from excessive filter

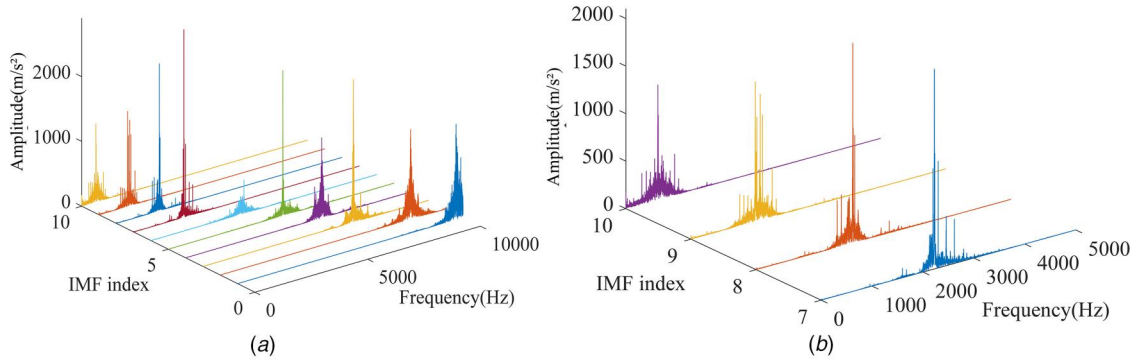

Fig. 5 (*a*) The decomposed IMFs by VMD and (*b*) residual IMFs after center frequency filtering

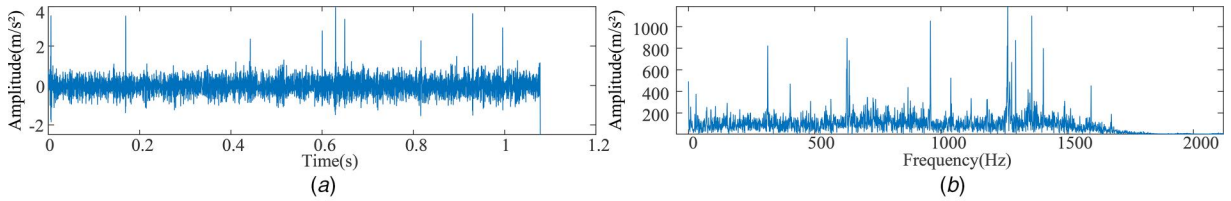

Fig. 6 (*a*) Time domain of the signal after bandpass filtering and (*b*) frequency domain of the signal after bandpass filtering

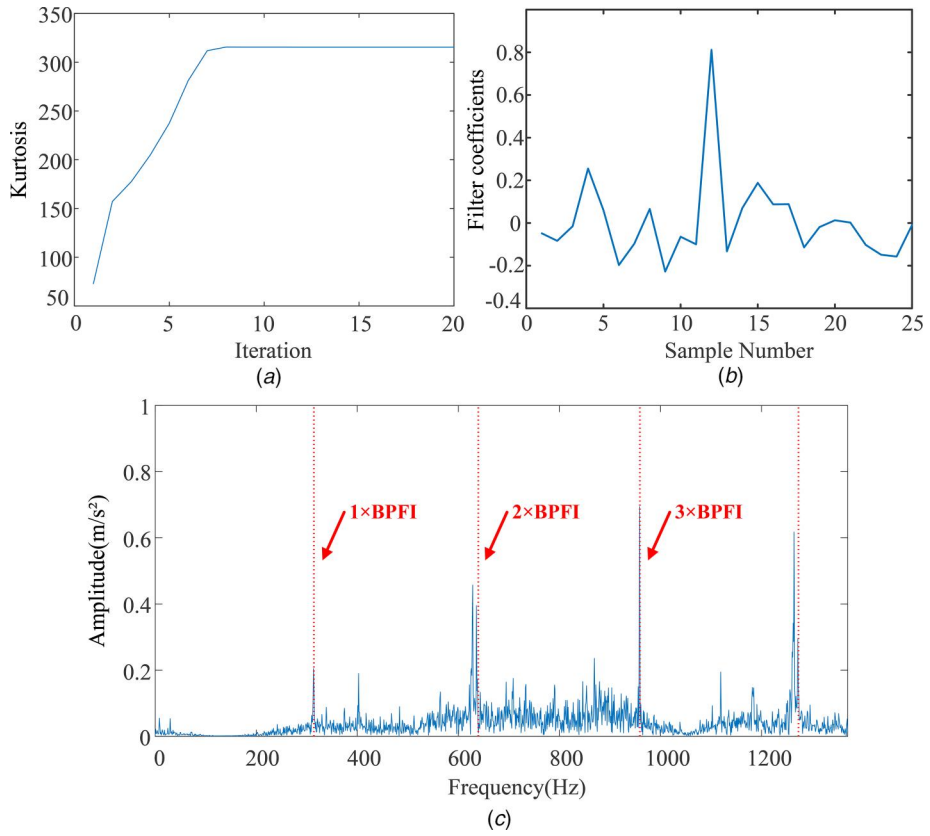

Fig. 7 (*a*) Changes in SK during iteration, (*b*) spectrum filter coefficients, and (*c*) the filtered amplitude spectrum

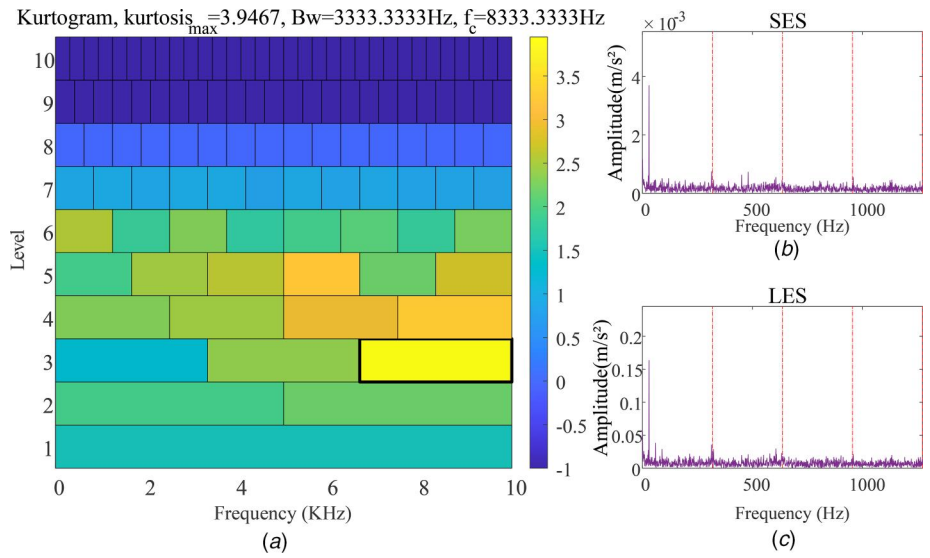

Fig. 8 (*a*) Demodulation band selection through Kurtogram, (*b*) squared envelope spectrum, and (*c*) logarithmic envelope spectrum

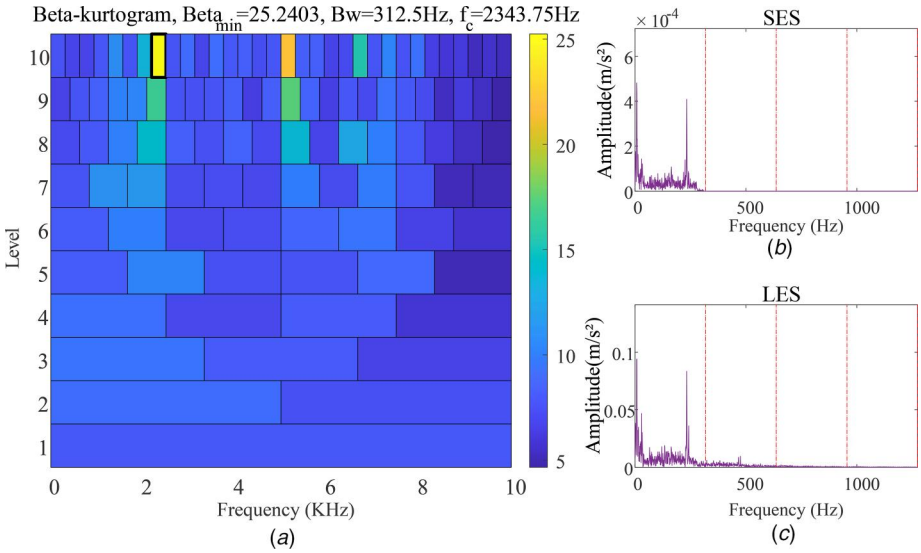

Fig. 9 (*a*) Demodulation band selection through Beta-Kurtogram, (*b*) squared envelope spectrum, and (*c*) logarithmic envelope spectrum

lengths. Such overfitting scenarios might inadvertently distort the amplitude spectrum's structural integrity and render the deconvolution process particularly susceptible to noise interference. Moreover, this controlled filter length helps prevent the erroneous interpretation of harmonic noise peaks as legitimate impulsive components, thereby enhancing the overall robustness of the methodology.

The iterative optimization process exhibited a distinctive pattern wherein the spectral kurtosis demonstrated a clear and consistent upward trajectory, as evidenced in Fig. 7(*a*). The culmination of this iterative process yielded a set of optimized filter coefficients, which are thoroughly documented in Fig. 7(*b*). After obtaining the filter coefficients through an iterative process, we apply a causal FIR filter. This method ensures that the output sequence length matches the input sequence length. We focus exclusively on frequency-domain amplitude characteristics and do not consider phase distortion. Because the filter has linear phase with a constant group delay of $(L-1)/2$ samples, the amplitude $Y(k)$ at frequency index k equals the amplitude $U(k)$ of the original spectrum at the same index, scaled by the filter's impulse response. As a result, the index positions of fault characteristic frequencies remain aligned before and after filtering. Boundary effects only influence the absolute amplitude values and do not alter the frequency indices.

The final stage of the analysis involved the application of the trained filter to the original signal, resulting in a filtered amplitude spectrum that reveals several significant findings. As illustrated in Fig. 7(*c*), the analysis demonstrates a pronounced concentration of energy at the rolling bearing fault characteristic frequency (BPFI = 319.769 Hz). The clear identification of both the fundamental frequency and its associated harmonic components provides compelling evidence for the method's effectiveness in extracting periodic impulsive features. Furthermore, this enhanced filtering strategy significantly improves the detectability of weak fault signatures within the frequency domain, thereby establishing a robust foundation for accurate fault classification and diagnosis in practical applications.

To further underscore the robustness and efficacy of the method proposed in this study, we conduct a comparative analysis of its performance against three established algorithms: the Kurtogram [32], the Beta-Kurtogram [5], and the Autogram [8]. The results of

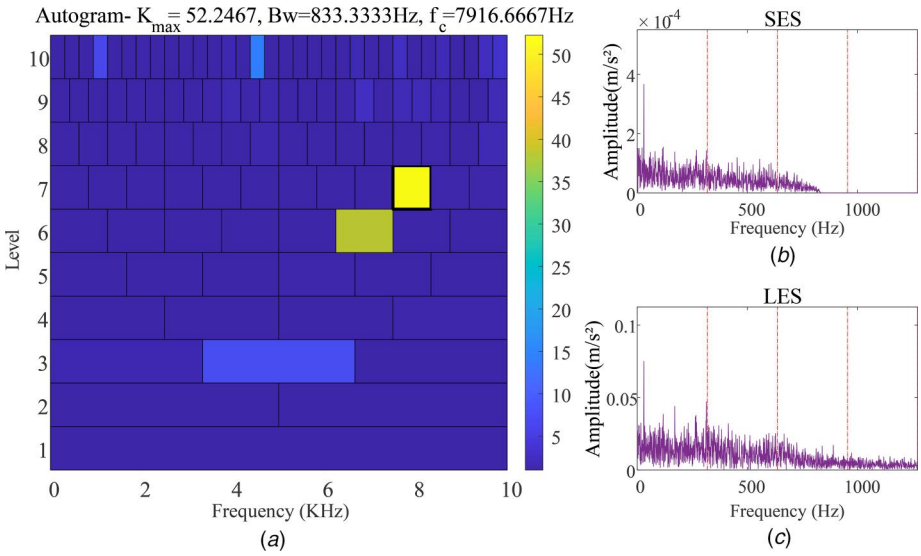

Fig. 10 (*a*) Demodulation band selection through Autogram, (*b*) squared envelope spectrum, and (*c*) logarithmic envelope spectrum

the signal processing conducted using these algorithms, alongside their respective limitations, are summarized and deliberated upon as follows.

The Kurtogram, as shown in Fig. 8(*a*), selects a filtering frequency band in the range of (6666.666 Hz, 9999.999 Hz) for analyzing the vibration signal. However, the output generated is suboptimal, as demonstrated by the squared envelope spectrum and the logarithmic squared envelope spectrum results depicted in Figs. 8(*b*) and 8(*c*), respectively. Neither spectrum exhibits prominent peaks corresponding to the characteristic fault frequencies of the bearing's inner ring or their harmonics. This lack of distinct spectral features highlights the inability of the Kurtogram method to adequately characterize the inner ring fault patterns, thus limiting its effectiveness in accurately diagnosing faults under the conditions tested.

Similarly, the Beta-Kurtogram also fails to provide a reliable characterization of the fault features. As illustrated in Fig. 9(*a*), the selected filtering frequency band lies between (2187.5 Hz, 2500 Hz). However, the analysis of the squared envelope spectrum and the logarithmic squared envelope spectrum, depicted in Figs. 9(*b*) and 9(*c*), respectively, reveals no discernable peaks at the bearing fault characteristic frequencies or their harmonics. The absence of such critical features in the processed signals indicates that the Beta-Kurtogram exhibits only limited effectiveness in detecting the fault characteristics of the system. In the case of the Autogram, the selected filtering frequency band is narrower, falling within the range of (7500 Hz, 8333.333 Hz), as shown in Fig. 10(*a*). Although the squared envelope spectrum of the filtered signal does not reveal any pronounced peaks at the characteristic fault frequencies or their harmonics, as observed in Fig. 10(*b*), the logarithmic squared envelope spectrum does exhibit a peak corresponding to the fundamental frequency of the BPFI, as shown in Fig. 10(*c*). Despite this minor indication of fault information, the Autogram largely fails to offer a comprehensive characterization of the fault features.

In contrast to the above results, the distinctive fault characteristics and their associated harmonics can be clearly and unambiguously identified in Fig. 8(*c*), which substantiates that our proposed methodological framework demonstrates remarkably robust performance. Furthermore, the approach successfully facilitates the precise identification of characteristic frequencies and their corresponding harmonics, as comprehensively illustrated in the aforementioned figure, thereby validating the method's enhanced diagnostic capabilities in fault detection scenarios.

5 Conclusion and Outlook

This research has successfully developed and validated EKBD-MK, an innovative diagnostic framework for wind turbine fault detection that addresses critical challenges in maintaining operational reliability. The framework's effectiveness is demonstrated through several key achievements. First, the integration of Shannon entropy-based noise quantification with center frequency interpretation has proven robust in complex noise environments, effectively handling the challenging mechanical and environmental conditions typical in wind turbine operations. Second, the implementation of VMD with an entropy-frequency dual-constraint system has shown superior capability in preserving fault information while maintaining signal integrity. Third, the adaptive blind deconvolution strategy, enhanced by spectral kurtosis and multicomponent preservation, has demonstrated significant improvements in fault feature extraction and noise suppression without parameter sensitivity issues. The experimental validation through case study confirms that EKBD-MK substantially outperforms existing methods in diagnostic precision, making it a valuable tool for wind turbine maintenance and reliability engineering. Furthermore, the EKBD-MK framework serves as a comprehensive diagnostic tool for rotating machinery impact failures, particularly excelling in complex industrial settings with mixed noise types through its dual-constraint filtering and collaborative noise suppression features. While successfully implemented in wind turbine bearing diagnostics with strong performance against speed variations and poor signal-to-noise ratios, the framework has limitations: it is restricted to rotating systems with periodic impact characteristics, requires high-precision sensors for ultralow-speed conditions, depends on prior fault frequency knowledge, involves complex computation, and has been validated only for specific bearing faults. The method shows potential for broader applications in rolling bearings, gearboxes, and high-speed rotors, though future development should focus on adaptive frequency estimation and expanded validation across diverse fault types and noise scenarios.

Funding Data

- National Natural Science Foundation of China (Grant Nos. 52105111 and 52305085; Funder ID: 10.13039/501100001809).
- Guangdong Basic and Applied Basic Research Foundation (Grant No. 2025A1515012256; Funder ID: 10.13039/501100021171).
- Shantou University (STU) Scientific Research Initiation Grant (No. NTF21029; Funder ID: 10.13039/100009047).
- Industry-Academia Cooperation Project from the Guangdong Institute of Special Equipment Inspection and Research Shunde Branch (XTJ-KY01-202503-030).
- Enterprise Collaboration Project from the National Excellent Engineer Innovation Research Institute for Advanced Manufacturing Industry in Foshan of Guangdong-Hong Kong-Macao Greater Bay Area (NSJH2025008).

Data Availability Statement

The datasets generated and supporting the findings of this article are obtainable from the corresponding author upon reasonable request.

References

[1] Chen, R., Gu, Y., Huang, P., Chen, J., and Qiu, G., 2024, "A Hierarchical Fault Diagnosis Model for Planetary Gearbox With Shift-Invariant Dictionary and OMPAN," ASME ASCE-ASME J. Risk Uncertainty Eng. Syst., Part B: Mech. Eng., **10**(3), p. 031101.

[2] Xin, G., Zhong, Q., Jin, Y., Li, Z., Chen, Y., Li, Y.-F., and Antoni, J., 2024, "Autonomous Bearing Fault Diagnosis Based on Fault-Induced Envelope Spectrum and Moving Peaks-Over-Threshold Approach," IEEE Trans. Instrum. Meas., **73**, pp. 1–12.

[3] Chen, P., Ma, Z., Xu, C., Jin, Y., and Zhou, C., 2024, "Self-Supervised Transfer Learning for Remote Wear Evaluation in Machine Tool Elements With Imaging Transmission Attenuation," IEEE Internet Things J., **11**(13), pp. 23045–23054.

[4] Chen, P., Ma, J., He, C., Jin, Y., and Fan, S., 2025, "Semi-Supervised Consistency Models for Automated Defect Detection in Carbon Fiber Composite Structures With Limited Data," Meas. Sci. Technol., **36**(4), p. 046109.

[5] Chen, P., Wu, Y., Fan, S., He, C., Jin, Y., Qi, J., and Zhou, C., 2025, "Adaptive Signal Regime for Identifying Transient Shifts: A Novel Approach Toward Fault Diagnosis in Wind Turbine Systems," Ocean Eng., **325**, p. 120798.

[6] Peng, D., Yazdanianasr, M., Mauricio, A., Verwimp, T., Desmet, W., and Gryllias, K., 2025, "Physics-Driven Cross Domain Digital Twin Framework for Bearing Fault Diagnosis in Non-Stationary Conditions," Mech. Syst. Signal Process., **228**, p. 112266.

[7] Chen, P., Zhang, R., He, C., Jin, Y., Fan, S., Qi, J., Zhou, C., and Zhang, C., 2025, "Progressive Contrastive Representation Learning for Defect Diagnosis in Aluminum Disk Substrates With a Bio-Inspired Vision Sensor," Expert Syst. Appl., **289**, p. 128305.

[8] Chen, P., Wu, Y., Xu, C., Huang, C.-G., Zhang, M., and Yuan, J., 2025, "Interference Suppression of Nonstationary Signals for Bearing Diagnosis Under Transient Noise Measurements," IEEE Trans. Reliab., pp. 1–15.

[9] Huang, C.-G., Huang, H.-Z., Li, Y.-F., and Peng, W., 2021, "A Novel Deep Convolutional Neural Network-Bootstrap Integrated Method for RUL Prediction of Rolling Bearing," J. Manuf. Syst., **61**, pp. 757–772.

[10] Chen, P., Gao, J., Zhang, R., Jin, Y., Yu, R., He, C., and Qi, J., 2025, "Metric-Guided Graph Contrastive Learning: An Unsupervised Approach for Few-Shot Gearbox Fault Diagnosis," Meas. Sci. Technol., **36**(7), p. 076110.

[11] Antoni, J., and Randall, R. B., 2006, "The Spectral Kurtosis: Application to the Vibratory Surveillance and Diagnostics of Rotating Machines," Mech. Syst. Signal Process., **20**(2), pp. 308–331.

[12] Qi, J., Kong, Y., Lv, Y., Lin, C., Han, Q., Zhang, X., Rao, M., Dong, M., Zuo, M. J., and Chu, F., 2025, "Order Spectrum-Assisted Sparse Learning Classification

Approach for Wind Turbine Drivetrain Fault Diagnostics Under Variable Operating Conditions," Renewable Energy, **253**, p. 123659.
[13] Antoni, J., 2007, "Fast Computation of the Kurtogram for the Detection of Transient Faults," Mech. Syst. Signal Process., **21**(1), pp. 108–124.
[14] Lei, Y., Lin, J., He, Z., and Zi, Y., 2011, "Application of an Improved Kurtogram Method for Fault Diagnosis of Rolling Element Bearings," Mech. Syst. Signal Process., **25**(5), pp. 1738–1749.
[15] Li, C., Cabrera, D., De Oliveira, J. V., Sanchez, R.-V., Cerrada, M., and Zurita, G., 2016, "Extracting Repetitive Transients for Rotating Machinery Diagnosis Using Multiscale Clustered Grey Infogram," Mech. Syst. Signal Process., **76–77**, pp. 157–173.
[16] Moshrefzadeh, A., and Fasana, A., 2018, "The Autogram: An Effective Approach for Selecting the Optimal Demodulation Band in Rolling Element Bearings Diagnosis," Mech. Syst. Signal Process., **105**, pp. 294–318.
[17] Zhou, Y., Kumar, A., Parkash, C., Vashishtha, G., Tang, H., Glowacz, A., Dong, A., and Xiang, J., 2023, "Development of Entropy Measure for Selecting Highly Sensitive WPT Band to Identify Defective Components of an Axial Piston Pump," Appl. Acoust., **203**, p. 109225.
[18] Yan, T., Wang, D., Xia, T., Zheng, M., Peng, Z., and Xi, L., 2023, "Entropy-Maximization Oriented Interpretable Health Indicators for Locating Informative Fault Frequencies for Machine Health Monitoring," Mech. Syst. Signal Process., **198**, p. 110461.
[19] Lei, Y., Lin, J., He, Z., and Zuo, M. J., 2013, "A Review on Empirical Mode Decomposition in Fault Diagnosis of Rotating Machinery," Mech. Syst. Signal Process., **35**(1–2), pp. 108–126.
[20] McDonald, G. L., Zhao, Q., and Zuo, M. J., 2012, "Maximum Correlated Kurtosis Deconvolution and Application on Gear Tooth Chip Fault Detection," Mech. Syst. Signal Process., **33**, pp. 237–255.
[21] Li, J., Liu, Y., and Xiang, J., 2023, "Optimal Maximum Cyclostationary Blind Deconvolution for Bearing Fault Detection," IEEE Sens. J., **23**(14), pp. 15975–15987.
[22] Wang, Z., Zhou, J., Du, W., Lei, Y., and Wang, J., 2022, "Bearing Fault Diagnosis Method Based on Adaptive Maximum Cyclostationarity Blind Deconvolution," Mech. Syst. Signal Process., **162**, p. 108018.
[23] Yi, Z., Pan, N., and Guo, Y., 2018, "Mechanical Compound Faults Extraction Based on Improved Frequency Domain Blind Deconvolution Algorithm," Mech. Syst. Signal Process., **113**, pp. 180–188.
[24] He, W., Qin, L., and Lu, Y., 2025, "Maximum Fourier Spectrum Cyclostationarity Blind Deconvolution and Its Application in Structural Health Monitoring of Power Transformers," Meas. Sci. Technol., **36**(1), p. 016120.
[25] Gille, M., Beaurepaire, P., Gayton, N., Dumas, A., and Yalamas, T., 2025, "Statistical Approaches for the Reduction of Measurement Errors in Metrology," ASME ASCE-ASME J. Risk Uncertainty Eng. Syst., Part B: Mech. Eng., **11**(2), p. 021201.
[26] Dragomiretskiy, K., and Zosso, D., 2014, "Variational Mode Decomposition," IEEE Trans. Signal Process., **62**(3), pp. 531–544.
[27] Hashim, S., and Shakya, P., 2023, "A Spectral Kurtosis Based Blind Deconvolution Approach for Spur Gear Fault Diagnosis," ISA Trans., **142**, pp. 492–500.
[28] Zhang, Z., Wang, J., Li, S., Han, B., and Jiang, X., 2023, "Fast Nonlinear Blind Deconvolution for Rotating Machinery Fault Diagnosis," Mech. Syst. Signal Process., **187**, p. 109918.
[29] Wang, S., Xiang, J., Tang, H., Liu, X., and Zhong, Y., 2019, "Minimum Entropy Deconvolution Based on Simulation-Determined Band Pass Filter to Detect Faults in Axial Piston Pump Bearings," ISA Trans., **88**, pp. 186–198.
[30] Zhang, Y. L., Zhang, Q. Y., and Melodia, T., 2010, "A Frequency-Domain Entropy-Based Detector for Robust Spectrum Sensing in Cognitive Radio Networks," IEEE Commun. Lett., **14**(6), pp. 533–535.
[31] Sacchi, M. D., Velis, D. R., and Cominguez, A. H., 1994, "Minimum Entropy Deconvolution With Frequency-Domain Constraints," Geophysics, **59**(6), pp. 938–945.
[32] Chen, P., Wu, Y., Xu, C., Jin, Y., and Zhou, C., 2024, "Markov Modeling of Signal Condition Transitions for Bearing Diagnostics Under External Interference Conditions," IEEE Trans. Instrum. Meas., **73**, pp. 1–8.